AIAA JOURNAL
Vol. 35, No. 8, August 1997

Control of Cantilever Vibration via Structural Tailoring and Adaptive Materials

L. Librescu,* L. Meirovitch,† and S. S. Na‡
Virginia Polytechnic Institute and State University, Blacksburg, Virginia 24061-0219

A dual approach integrating structural tailoring and adaptive materials technology and designed to control the dynamic response of cantilever beams subjected to external excitations is presented. Whereas structural tailoring uses the anisotropy properties of advanced composite materials, adaptive materials technology exploits the actuating capabilities of piezoelectric materials bonded or embedded into the host structure. A control law relating the piezoelectrically induced boundary bending moment with the velocity at given points of the structure is implemented and its effect on the closed-loop frequencies and dynamic response to harmonic excitations is investigated. The combination of structural tailoring and control by means of adaptive materials proves very effective in damping out vibration.

I. Introduction

As the requirements for higher flexibility on high-speed aircraft increase, so do the challenges of developing innovative design solutions. Whereas the increased flexibility is likely to provide enhanced aerodynamic performance, the aircraft also must be able to fulfill a multitude of missions in complex environmental conditions and to feature an expanded operational envelope and longer operational life. To achieve such ambitious goals—advanced concepts resulting in the enhancement of static and dynamic response of the multimission—highly flexible aircraft must be developed and implemented. One way of achieving such goals consists of the integration of advanced composite materials in the aircraft structure.[1] In this regard, the directionality property featured by anisotropic composite materials is capable of providing the desired elastic couplings through the proper selection of the ply angle. However, such a technique is passive in nature in the sense that, once the design is in place, the structure cannot respond to the variety of conditions in which it must operate.

The situation can be mitigated by incorporating into the host structure adaptive materials able to respond actively to changing conditions. In a structure with adaptive capabilities, the natural frequencies, damping, and mode shapes can be tuned to reduce the vibration so as to avoid structural resonance and flutter instability, and in general to enhance the dynamic response characteristics. The adaptive capability is achieved through the converse piezoelectric effect, which consists of the generation of localized strains in response to an applied voltage. This induced strain field produces, in turn, a change in the dynamic response characteristics of the structure. It is proposed here to enhance the free vibration and dynamic response to external excitations of wing structures by incorporating the adaptive capability referred to as induced strain actuation in conjunction with structural tailoring. Under consideration is a cantilevered aircraft wing, modeled as a thin/thick-walled closed cross-section beam of anisotropic material. Implementation of a control law relating the applied electric field to one of the mechanical quantities characterizing the response of the wing according to a prescribed functional relationship results in eigenvalue/boundary-value problems. The solution consists of closed-loop eigenvalues/dynamic response characteristics, which are functions of the applied voltage, i.e., of the feedback control gain.

Investigation of static and dynamic control of aircraft wing structures via the simultaneous implementation of induced strain actuation and structural tailoring is of recent vintage. Among the few investigations using both techniques, we single out two.[2,3] The present study, consistent with some approaches,[4,5] represents a clear departure from other approaches[3,6,7] in the sense that here a dynamic feedback control strategy is implemented. This enables us to control the free and forced vibrations and avoid the resonance phenomenon without weight penalties. Moreover, this adaptive strategy promises to be effective also in flutter control.

Although the paper addresses mainly the problem of control of aircraft wings, the concept transcends this application. This implies that the methodology developed here can be applied to a number of other advanced structures. Indeed, the approach is applicable to other lightweight structural models, such as helicopter blades and flexible robot arms operating in space.

II. Basic Assumptions and Kinematics

The structural model used here consists of a cantilevered thin-walled, closed-section beam. Its purpose is to simulate the lifting surface of advanced flight vehicles. The model is confined to uniform single-cell beams. Two systems of coordinates, s, z, n and x, y, z, are used to define points of the thin-walled beam (Fig. 1). Note that the z axis is located so as to coincide with the axis of symmetry of the cross-sectional areas. The beam model incorporates the following nonclassical features: 1) anisotropy of the constituent material layers; 2) transverse shear; 3) nonuniform torsion, in the sense that the rate of twist $\mathrm{d}\Theta/\mathrm{d}z$ is no longer assumed to be constant (as in the Saint-Venant torsional model) but a function of the spanwise coordinate; and 4) primary and secondary warping effects. We also postulate in-plane cross-section nondeformability of the beam. In view of these features and assumptions, the present beam model is capable of providing results also for thick-walled beams and/or for constituent materials exhibiting high flexibilities in transverse shear.

In accordance with these assumptions and to reduce the three-dimensional problem to an equivalent one-dimensional one, the x, y, z components of the displacement vector are expressed as[8–10]

$$u(x, y, z, t) = u_o(z, t) - y\Theta(z, t) \tag{1a}$$

$$v(x, y, z, t) = v_o(z, t) + x\Theta(z, t) \tag{1b}$$

$$w(x, y, z, t) = w_o(z, t) + \theta_x(z, t)\left[y(s) - n\frac{\mathrm{d}x}{\mathrm{d}s}\right] + \theta_y(z, t)\left[x(s) + n\frac{\mathrm{d}y}{\mathrm{d}s}\right] - \Theta'(z, t)\left[F_\omega(s) + na(s)\right] \tag{1c}$$

where $\Theta'(z, t)$ represents the torsion-related warping measure,

$$\theta_x(z, t) = \gamma_{yz}(z, t) - v_o'(z, t) \tag{2a}$$

Received Nov. 16, 1995; revision received Jan. 9, 1997; accepted for publication April 14, 1997.

*Professor, Department of Engineering Science and Mechanics.
†University Distinguished Professor, Department of Engineering Science and Mechanics. Fellow AIAA.
‡Graduate Student, Department of Engineering Science and Mechanics.

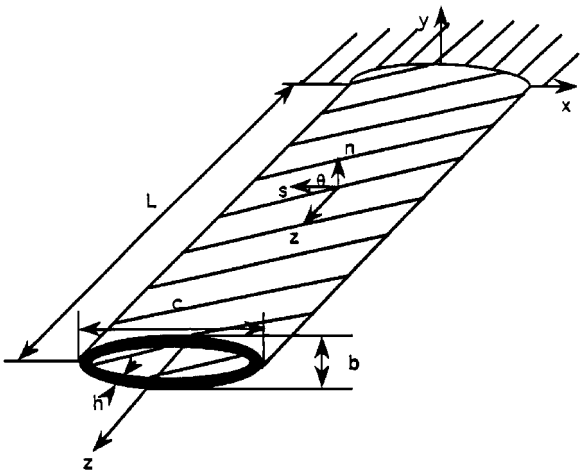

Fig. 1 Geometry of wing structure: L = 80 in. (2.032 m), c = 10 in. (0.254 m), b = 2.68 in. (0.06807 m), and h = 0.4 in. (0.01016 m).

$$\theta_y(z,t) = \gamma_{xz}(z,t) - u_o'(z,t) \tag{2b}$$

and

$$a(s) = -y(s)\frac{dy}{ds} - x(s)\frac{dx}{ds} \tag{2c}$$

in which $\theta_x(z,t)$ and $\theta_y(z,t)$ denote the rotations about axes x and y, respectively, and γ_{yz} and γ_{xz} denote the transverse shear strains in the planes yz and xz, respectively; primes denote derivatives with respect to the z coordinate. When the transverse shear effect is ignored, $\theta_x \to -v_o'$ and $\theta_y \to -u_o'$. Equations (1) and (2) reveal that six kinematic variables, $u_o(z,t)$, $v_o(z,t)$, $w_o(z,t)$, $\theta_x(z,t)$, $\theta_y(z,t)$, and $\Theta(z,t)$, representing three translations in the x, y, and z directions and three rotations about the x, y, and z axes, respectively, are used to define the displacement components u, v, and w. The primary warping function has the expression[8,9]

$$F_\omega(s) = \int_o^s [r_n(s) - \psi]\, ds \tag{3}$$

where

$$\psi = \frac{\oint_C [r_n(s)/h(s)]\, ds}{\oint_C [1/h(s)]\, ds} \tag{4}$$

is the torsional function, in which the quantity $h(s)$ denotes the beam wall thickness, allowed to vary along the periphery,

$$\oint_C (\,)\, ds$$

denotes the integral around the entire periphery C of the midline cross section of the beam, and

$$r_n(s) = x(s)\frac{dy}{ds} - y(s)\frac{dx}{ds} \tag{5}$$

Note that

$$\int_o^s r_n(s)\, ds$$

is referred to as the sectorial area $\Omega(s)$. For the case of uniform h in the circumferential direction, Eq. (4) reduces to $\psi = 2A_C/\beta$, where A_C denotes the cross-sectional area bounded by the midline and β denotes the total length of the contour midline.

Using the kinematic representation given by Eqs. (1) and (2), one can obtain the two-dimensional strain measures

$$\epsilon_{zz}^0(s,z,t) = w_0' + x(s)\theta_y' + y(s)\theta_x' - F_\omega(s)\Theta'' \tag{6a}$$

$$\epsilon_{zz}^n(s,z,t) = \theta_y'\frac{dy}{ds} - \theta_x'\frac{dx}{ds} - a(s)\Theta'' \tag{6b}$$

$$\gamma_{sz}^0(s,z,t) = (u_0' + \theta_y)\frac{dx}{ds} + (v_0' + \theta_x)\frac{dy}{ds} + 2\frac{A_C}{\beta}\Theta' \tag{6c}$$

$$\gamma_{sz}^n(s,z,t) = 2n\Theta' \tag{6d}$$

$$\gamma_{zn}(s,z,t) = (u_0' + \theta_y)\frac{dy}{ds} - (v_0' + \theta_x)\frac{dx}{ds} \tag{6e}$$

where ϵ_{zz}^0 and ϵ_{zz}^n denote the axial strain components associated with the primary and secondary warping, γ_{sz}^0 and γ_{sz}^n denote the membrane shear and the thicknesswise shear induced by the secondary warping, respectively, and γ_{zn} denotes the transverse shear strain.

III. Location of Piezoactuator Patches: Global Constitutive Equations

We assume that the master structure consists of m layers and the actuator of l piezoelectric layers and that the actuators are distributed over the entire span of the beam. Along the circumferential s and transverse n directions, they are distributed according to

$$\begin{aligned} R_{(k)}(n) &= H[n - n_{(k-)}] - H[n - n_{(k+)}] \\ R_{(k)}(s) &= H[s - s_{(k-)}] - H[s - s_{(k+)}] \end{aligned} \tag{7}$$

where R is a spatial function and $H[\,]$ denotes the Heaviside distribution, in which the subscript k in parentheses identifies the kth layer. The linear constitutive equations for a three-dimensional piezoelectric continuum, expressed in Voigt's contracted notation, are[11]

$$\sigma_i = C_{ij}^{\mathcal{E}} S_j - e_{ri}\mathcal{E} \tag{8a}$$

$$D_r = e_{rj}S_j + \varepsilon_{rl}^S \mathcal{E} \tag{8b}$$

in which summation over repeated indices is implied. Moreover, σ_i and S_j ($i, j = 1, 2, \ldots, 6$) denote the stress and strain components, respectively, where

$$S_j = \begin{cases} S_{pr}, & p = r, \quad j = 1, 2, 3 \\ 2S_{pr}, & p \neq r, \quad j = 4, 5, 6 \end{cases} \tag{9}$$

Moreover, $C_{ij}^{\mathcal{E}}$, e_{ri}, and ε_{rl}^S are the elastic (measured for conditions of a constant electric field), piezoelectric, and dielectric constants (measured under constant strain) and $\mathcal{E}$ and D_r ($r = 1, 2, 3$) denote the electric-field intensity and electric displacement vector, respectively. Whereas Eq. (8a) describes the converse piezoelectric effect, consisting of the generation of mechanical stress or strain in response to an electric field, Eq. (8b) describes the direct piezoelectric effect, consisting of the generation of an electrical charge under a mechanical force. In adaptive structures, the direct effect is used for sensing and the converse effect is used for active control. Equations (8) are valid for the most general case of anisotropy, i.e., for triclinic crystals. In the following, we restrict ourselves to an in-plane isotropic piezoelectric continuum. In this case, the piezoelectric continuum is characterized by five independent elastic coefficients, $C_{11} = C_{22}$, $C_{13} = C_{23} = C_{31} = C_{32}$, C_{33}, $C_{44} = C_{55}$, and $C_{66} \equiv (C_{11} - C_{12})/2$; three independent piezoelectric coefficients, $e_{15} = e_{24}$, $e_{31} = e_{32}$, and e_{33}; and two independent dielectric constants, $\varepsilon_{11} = \varepsilon_{22}$, ε_{33} (Ref. 11).

At this point, we assume that the master structure is made of anisotropic material layers, the anisotropy being of the monoclinic type. We also assume that the electric-field vector $\mathcal{E}$ is represented in terms of the component $\mathcal{E}_3$ only, implying that $\mathcal{E}_1 = \mathcal{E}_2 = 0$. As a result of the uniform voltage distribution, $\mathcal{E}_3$ depends on time alone and is independent of the spatial position. Invoking the stipulated distribution law of piezoactuators, Eqs. (7), and the specific anisotropy properties, the three-dimensional constitutive equations for the actuator layers can be expressed as

$$\begin{bmatrix} \sigma_{ss} \\ \sigma_{zz} \\ \sigma_{sz} \end{bmatrix}_{(k)} = \begin{bmatrix} C_{11} & C_{12} & 0 \\ C_{12} & C_{11} & 0 \\ 0 & 0 & \dfrac{C_{11} - C_{12}}{2} \end{bmatrix}_{(k)} \begin{bmatrix} S_{ss} \\ S_{zz} \\ S_{sz} \end{bmatrix}_{(k)} - \begin{bmatrix} e_{31}^{(k)}\mathcal{E}_3^{(k)} R_k(n) R_k(s) \\ e_{31}^{(k)}\mathcal{E}_3^{(k)} R_k(n) R_k(s) \\ 0 \end{bmatrix} \tag{10a}$$

and

$$\sigma_{nz}^{(k)} = C_{44}^{(k)} S_{nz}^{(k)} \tag{10b}$$

The last terms in Eq. (10a) identify the actuation stresses induced by the applied electric field. Integrating the three-dimensional constitutive equations through the thickness of the master structure and actuators and postulating that the hoop stress resultant N_{ss} is negligibly small when compared with the remaining stresses, two-dimensional constitutive equations (referred to also as shell-constitutive equations) are obtained. The equations are displayed in the Appendix.

IV. Boundary-Value Problem Involving Bending-Twist Coupling

The great possibilities provided by advanced anisotropic composite materials can be used to enhance the response of lifting surfaces. Implementation of structural/aeroelastic tailoring has revealed great promise toward improving static and dynamic response characteristics, preventing vibration resonance and enhancing aeroelastic behavior. For thin-walled composite beams, tailoring was carried out in a number of recent papers[3,8–10] in which the possibility of generating desired elastic couplings beneficial to specific aeronautical problems was examined. Among the possible couplings that can be induced via tailoring, the most beneficial for the problem at hand is the bending-twist cross coupling. This coupling also has been used for the solid beam model to enhance the structural/aeroelastic response behavior of wing structures.[1,12–15] As shown elsewhere,[16,17] the ply-angle distribution with respect to the spanwise z axis inducing such a cross coupling is

$$\theta(y) = -\theta(-y) \tag{11}$$

Using such a ply angle, the equations of motion for cantilever beams are[9,10]

$$a_{55}(v_o'' + \theta_x') + \underline{\underline{a_{56}}}\Theta''' + p_y = b_1\ddot{v}_o \tag{12a}$$

$$\underline{\underline{a_{66}}}\Theta'''' + a_{77}\Theta'' - a_{56}(v_o''' + \theta_x'') + a_{73}\theta_x''' + m_z = (b_4 + b_5)\ddot{\Theta} - \underline{\underline{(b_{10} + b_{18})}}\ddot{\Theta}'' \tag{12b}$$

$$a_{33}\theta_x'' + a_{37}\Theta'' - a_{55}(v_o' + \theta_x) - \underline{\underline{a_{56}}}\Theta'' = \underline{(b_4 + b_{14})\ddot{\theta}_x} \tag{12c}$$

which are subject to the geometric boundary conditions at $z = 0$,

$$v_o = 0 \tag{13a}$$

$$\theta_x = 0 \tag{13b}$$

$$\Theta = 0 \tag{13c}$$

$$\underline{\underline{\Theta'}} = 0 \tag{13d}$$

and the natural boundary conditions at $z = L$,

$$a_{55}(v_o' + \theta_x) + \underline{\underline{a_{56}}}\Theta'' = 0 \tag{14a}$$

$$a_{33}\theta_x' + a_{37}\Theta' = \hat{M}_x \tag{14b}$$

$$\underline{\underline{a_{66}}}\Theta''' + a_{77}\Theta' - a_{56}(v_o'' + \theta_x') + a_{37}\theta_x' = -\underline{\underline{(b_{10} + b_{18})}}\ddot{\Theta}' \tag{14c}$$

$$a_{56}(v_o' + \theta_x) + \underline{\underline{a_{66}}}\Theta'' = 0 \tag{14d}$$

The terms underscored in Eqs. (12–14) by single and double dashed lines are associated with warping inhibition and warping inertia effect, respectively, whereas the terms underscored by a solid line or marked by a caret are associated with the rotatory inertia and the prescribed bending moment, respectively.

V. Vibration Control Through a Bending Moment at the Beam Tip

The interest lies in controlling the vibration of the beam by means of a bending moment at the tip.[18,19] Such a bending-moment control can be generated by incorporating piezoactuators into the structure and using the converse effect featured by these devices. Structures with embedded or bonded piezoactuators are referred to as intelligent structures. A comprehensive review and assessment of the state of the art in the use of intelligent structures for aerospace applications can be found elsewhere.[20]

As shown elsewhere,[3,6,7] piezoactuators featuring in-plane isotropic properties spread over the entire span of the beam and bonded symmetrically on the outer and inner faces of the beam, but activated out of phase, generate a bending moment at the beam tip in response to an electric field $\mathcal{E}$. For feedback control, the applied electric field $\mathcal{E}$ is related to one of the mechanical quantities characterizing the system response. This permits implementation of a number of control laws. The efficiency of these control laws can be measured in terms of their ability to enhance the free-vibration behavior, reducing the forced vibration to external excitations and preventing resonance.

A number of control laws have been proposed in conjunction with boundary-control moments.[3–7] Showing great promise is velocity feedback control used to control a classic solid beam.[4,5,21] For the problem at hand, the piezoelectrically induced tip moment $\hat{M}_x$ using velocity feedback control must be proportional to the rotational velocity $\dot{\theta}_x(L, t)$. A more explicit expression of this control law can be obtained from Eq. (14b) in the form

$$a_{33}\theta_x'(L, t) + a_{37}\Theta'(L, t) - k_p\dot{\theta}_x(L, t) = 0 \tag{15}$$

where k_p denotes the feedback control gain. Because of the presence of the term a_{37} in Eq. (15), it is clear that the boundary-control moment also can generate twist. The closed-loop boundary-value problem is obtained by replacing Eq. (14b) by Eq. (15).

VI. Numerical Examples

The equations derived in this paper are general, in the sense that they are valid for a beam of arbitrary cross section. However, in this paper, a biconvex profile, typical of supersonic aircraft wings, is adopted. Its geometric characteristics are displayed in Fig. 1. The piezoelectric actuators are mounted symmetrically on the top and bottom surfaces of the beam and they are made of PZT-4 piezoceramic with properties as given elsewhere.[22] The structure is assumed to be made of a graphite–epoxy composite material with the following properties:

$$E_L = (30 \times 10^6 \text{ psi})(20.68 \times 10^{10} \text{ N/m}^2)$$

$$E_T = (0.75 \times 10^6 \text{ psi})(5.17 \times 10^9 \text{ N/m}^2)$$

$$G_{LT} = (0.37 \times 10^6 \text{ psi})(2.25 \times 10^9 \text{ N/m}^2)$$

$$G_{TT} = (0.45 \times 10^6 \text{ psi})(3.10 \times 10^9 \text{ N/m}^2)$$

$$\mu_{TT} = \mu_{LT} = 0.25$$

$$\rho = (14.3 \times 10^{-5} \text{ lb s}^2/\text{in.}^4)(1528.15 \text{ kg/m}^3)$$

$$t_{\text{act}} = (0.78 \times 10^{-2} \text{ in.})(0.2 \times 10^{-3} \text{ m})$$

where the subscripts L and T denote directions parallel and transverse to the fibers, respectively, and t_{act} denotes the actuator thickness.

Combining structural tailoring and boundary moment control, two problems have been considered, namely, free vibration and harmonic excitation. In the case of free vibration, all field variables, denoted generically by $F(z, t)$, have the form

$$F(z, t) = \bar{F}(z)e^{\lambda t} \tag{16}$$

where the exponent λ is generally complex. Because λ appears in both the equations of motion and the boundary conditions, the solution of the corresponding eigenvalue problem tends to be complicated. In the second problem, the structure is excited by a concentrated harmonic load located at $z = z_0$. Concentrated loads can be represented as distributed as follows:

$$p_y(z, t) = F_0\delta(z - z_0)e^{i\omega t} \tag{17}$$

where F_0 is the amplitude, $\delta(z - z_0)$ a spatial Dirac delta function, and ω the excitation frequency. When p_y is located off the longitudinal axis of symmetry by an amount x_0, then it gives rise to the concentrated moment

$$m_z(z, t) = F_0x_0\delta(z - z_0)e^{i\omega t} \tag{18}$$

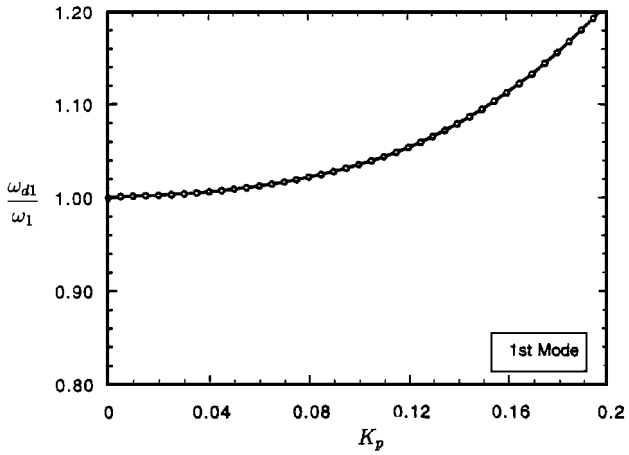

Fig. 2 First normalized damped frequency $\bar{\omega}_{d1}(\equiv \omega_{d1}/\bar{\omega}_1)$ vs dimensionless feedback gain for $AR = 16$, $\theta = 45$ deg, and $\bar{\omega}_1 = 55.31$ rad/s.

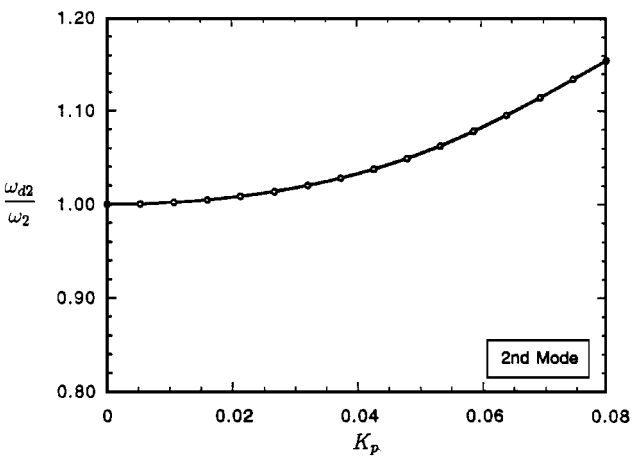

Fig. 3 Second normalized damped frequency $\bar{\omega}_{d2}(\equiv \omega_{d2}/\bar{\omega}_2)$ vs dimensionless feedback gain for $AR = 16$, $\theta = 45$ deg, and $\bar{\omega}_2 = 345.6$ rad/s.

For the free-vibration problem, it is necessary to solve the closed-loop eigenvalue problem. To this end, we introduce $\underline{v}_0(z,t) = \bar{v}_0(z)e^{\lambda t}$, $\theta_x(z,t) = \bar{\theta}_x(z)e^{\lambda t}$, and $\Theta(z,t) = \bar{\Theta}(z)e^{\lambda t}$ in Eqs. (11–14), with Eq. (14b) replaced by Eq. (15), divide through by $e^{\lambda t}$, and obtain a differential eigenvalue problem in $\bar{v}_0(z)$, $\bar{\theta}_x(z)$, and $\bar{\Theta}(z)$. Because the differential eigenvalue problem does not admit a closed-form solution, it is necessary to discretize it in the spatial variable. Because this is a non-self-adjoint problem, the indicated discretization procedure is the Galerkin method,[23] which amounts to expanding $\bar{v}_0(z)$, $\bar{\theta}_x(z)$, and $\bar{\Theta}(z)$ in series of trial functions satisfying all boundary conditions, multiplying Eqs. (12a), (12b), and (12c) by the same trial functions, in sequence, integrating over the structure and obtaining a nonsymmetric algebraic eigenvalue problem.[24] The difficulty with this approach lies in the requirement that the trial functions satisfy both the geometric and the natural boundary conditions. This difficulty can be circumvented by using a modified Galerkin method, whereby the discretization process is carried out directly in the extended Hamilton's principle.[23,25,26] Details of the approach are provided in the Appendix.

The solution of the algebraic eigenvalue problem derived in the Appendix yields the closed-loop eigenvalues

$$\frac{\lambda_r}{\bar{\lambda}_r} = \sigma_r \pm i\omega_{dr}, \qquad r = 1, 2, \ldots, n \tag{19}$$

which depend on the feedback control gain k_p and the ply angle θ, in addition to the system parameters, where σ_r is a measure of the damping in the rth mode and ω_{dr} is the rth frequency of damped oscillation. From Eqs. (19), we obtain the damping factor in the rth mode in the form

$$\zeta_r = -\frac{\sigma_r}{(\sigma_r^2 + \omega_{dr}^2)^{\frac{1}{2}}} \tag{20}$$

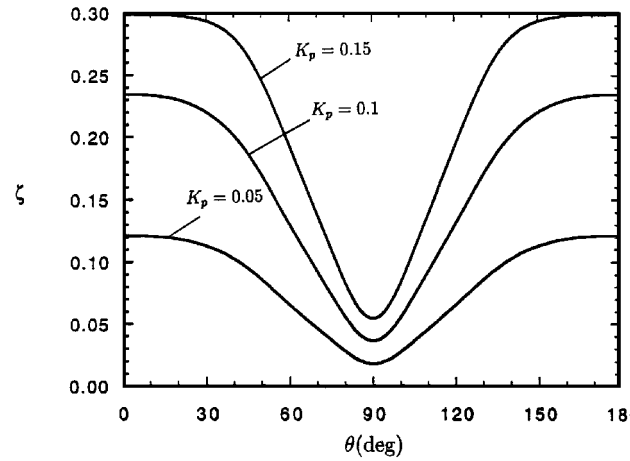

Fig. 4 Induced damping factor vs ply angle for various values of feedback gain.

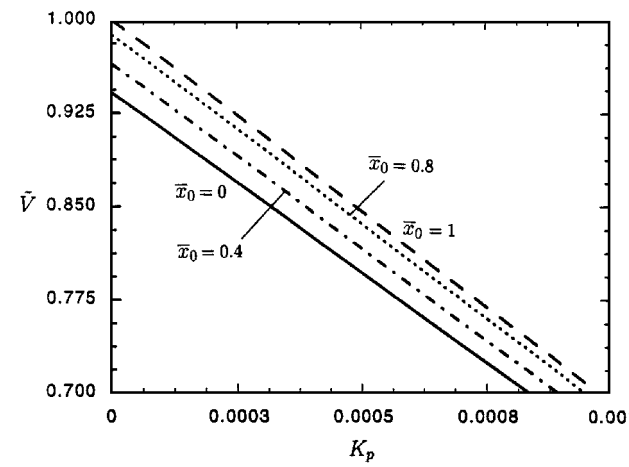

Fig. 5 Normalized deflection vs feedback gain for $AR = 16$ and $\theta = 60$ deg ($\bar{V} = V/\bar{V}$, $\bar{V} = 2 \times 10^5$ corresponds to $\bar{x}_0 = 1$ and $K_p = 0$).

Figures 2 and 3 show plots of the ratio ω_{dr}/ω_r vs the nondimensional feedback gain $K_p = k_p L\bar{\omega}/a_{33}$ for the first two modes and for the ply angle $\theta = 45$ deg, in which ω_r is the frequency of undamped oscillation corresponding to the uncontrolled structure and $\bar{\omega} = 40.33$ rad/s is an open-loop frequency corresponding to a free-warping, infinitely stiff-in-shear beam model with $\theta = 0$ deg and $AR = 16$. The plots show that the effect of the feedback control is smaller for the second mode than for the first.

Figure 4 depicts the induced damping factor ζ vs the ply angle θ for three different values of the feedback gain K_p. The plots are for $AR = 16$ and without transverse shear and warping restraint. In addition to the well-established fact that damping can be induced by feedback control, the plot reveals that tailoring can be used to increase damping in the structure as well.

Figure 5 depicts the normalized steady-state deflection due to a harmonic eccentric tip force as a function of the feedback gain with the normalized eccentricity $\bar{x}_0 = x_0/c$ acting as a parameter. The plots reveal the obvious trends that $\bar{V}$ increases with c and decreases with an increase in the control gain.

Figure 6 displays the normalized bending moment at the wing root vs the control gain with the ply angle as a parameter. The bending moment has a maximum for the value $\theta = 0$ of the ply angle, for which the bending stiffness a_{33} has a minimum, and a minimum for $\theta = 90$ deg, for which a_{33} has a maximum. This implies that tailoring and feedback control can be used in tandem to reduce the bending moment, thus avoiding overdesign at the root of the beam. Figure 6 also reveals that for relatively large values of the feedback gain, tailoring becomes less efficient than for low feedback gains. This suggests a tradeoff between the two techniques.

Figure 7 depicts the time history of the normalized deflection for the ply angle $\theta = 0$ for controlled and uncontrolled beams, with and without transverse shear and with warping restraint included.

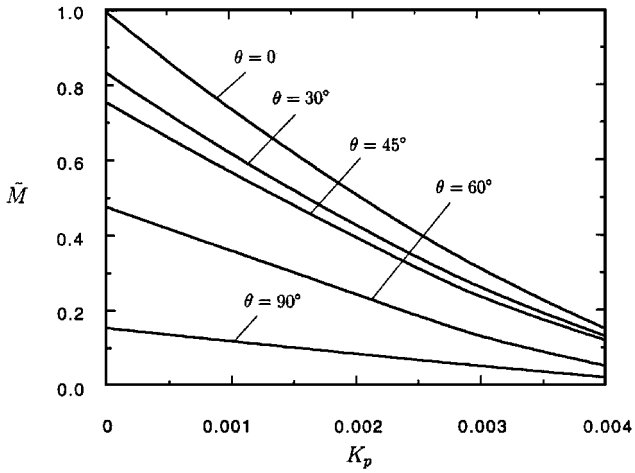

Fig. 6 Normalized bending moment at wing root vs feedback gain with ply angle as a parameter for $AR = 16$ ($\tilde{M} = M/\bar{M}$ and $\bar{M} = 432{,}583$ corresponds to $\theta = 0$ and $K_p = 0$).

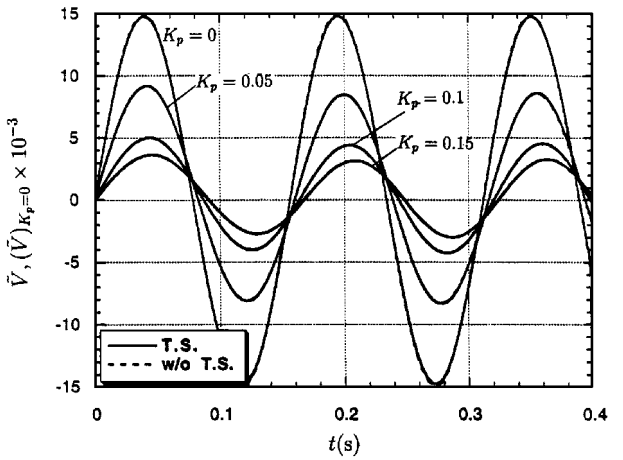

Fig. 7 Normalized deflection vs time for $AR = 16$ and $\theta = 0$.

As θ increases from 0 to 90 deg, the bending stiffness increases from a very low value to a maximum one and the displacement amplitude decreases at the same time. There is a significant increase in the response frequency from $\theta = 0$ to 90 deg. This is evidently because the bending stiffness experiences a dramatic increase when θ changes from 0 to 90 deg; the effectiveness of the control in reducing the vibration becomes obvious. One also can observe that, with an increase in K_p, a corresponding decrease in the slope of the curve is experienced. This corroborates the conclusion that in this case the maximum velocity decreases and damping increases. Results not displayed here reveal that, as θ increases from 0 to 90 deg, the bending stiffness increases and, consistent with this, the displacement decreases.

Finally, the mass and stiffness of the actuators were included in all numerical results obtained here. It is common practice, however, to ignore them, so that a comparison of results obtained by including and ignoring the mass and stiffness of actuators should prove of interest. Figure 8 shows such a study in the form of two sets of frequency response plots, the set in solid lines corresponding to the case in which the mass and stiffness of the actuators are considered and the dashed lines corresponding to the case in which they are not. As can be concluded from Fig. 8, the effect of ignoring the mass and stiffness of the actuators is to predict a resonance frequency about 10% smaller and response amplitudes higher than the actual ones. The case depicted in Fig. 8 seems to present a worse-than-average picture. In the other frequency response plots, the resonance frequency obtained by ignoring the mass and stiffness of the actuators (results not shown) was about 4–6% smaller. Moreover, results not displayed here reveal that transverse shear has the effect of reducing the resonance frequencies, whereas the warping restraint has the opposite effect. On the other hand, transverse shear tends to increase and warping restraint tends to decrease displacements.

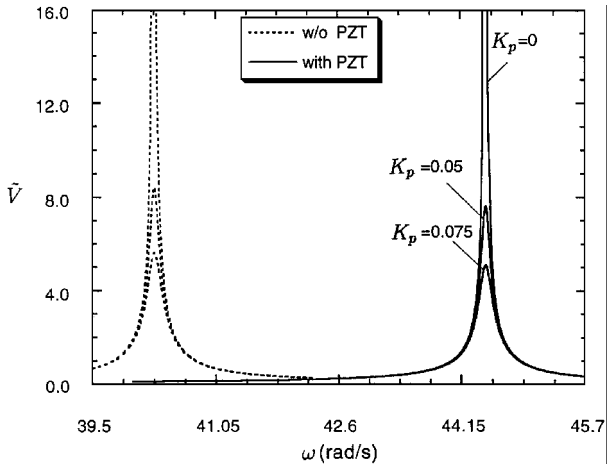

Fig. 8 Normalized deflection vs excitation frequency with and without mass and stiffness of actuators for shearable beam models with warping restraint and with $AR = 16$ and $\theta = 0$.

VII. Conclusions

A dual technology based on the use of structural tailoring and boundary-moment control aimed at enhancing the dynamic response characteristics of structures typical of aircraft wings was developed. The results reveal that, using the control law described in this paper in conjunction with the tailoring technique, a significant improvement in the dynamic response of thin-wall cantilever structures can be achieved.

The paper also highlights the importance of a number of nonclassic effects, such as anisotropy, transverse shear, and warping restraint, which strongly influence the dynamic response of advanced cantilever structures. As a matter of interest, a study of the effect of ignoring the mass and stiffness of the piezoelectric actuators also is presented.

Appendix: Derivation of Boundary-Value Problem and Eigenvalue Problem

The boundary-value problem can be derived by means of the extended Hamilton's principle,[23] which can be stated in the form

$$\int_{t_1}^{t_2} (\delta T - \delta V + \delta W)\, \mathrm{d}t = 0, \qquad \delta v_0 = 0$$
$$\delta\theta_x = 0, \qquad \delta\Theta = 0 \qquad \text{at} \qquad t = t_1, t_2 \tag{A1}$$

where T is the kinetic energy, V the potential energy, and δW the virtual work of the nonconservative forces. From previous work,[10] the kinetic energy is given by

$$T = \frac{1}{2}\int_0^L \oint \sum_{h(k)}^{N} \int \rho(k) \left\{ y^2 \dot{\Theta}^2 + (\dot{v}_0 + x\dot{\Theta})^2 + \left[(y\dot{\theta}_x - F_\omega \dot{\Theta}') - n\left(\frac{\mathrm{d}x}{\mathrm{d}s}\dot{\theta}_x + a\dot{\Theta}' \right) \right]^2 \right\} \mathrm{d}n\, \mathrm{d}s\, \mathrm{d}x \tag{A2}$$

and the potential energy has the form

$$V = \frac{1}{2}\int_0^L \oint \sum_{h(k)}^{N} \int \left\{ \sigma_{zz}^{(k)} \left[y\theta_x' - F_\omega \Theta'' - n\left(\frac{\mathrm{d}x}{\mathrm{d}s}\theta_x' + a\Theta'' \right) \right] + \sigma_{sz}^{(k)} \left[(v_0' + \theta_x)\frac{\mathrm{d}y}{\mathrm{d}s} + \frac{2A_C}{\beta}\Theta' \right] - \sigma_{nz}^{(k)} (v_0' + \theta_x)\frac{\mathrm{d}x}{\mathrm{d}s} \right\} \mathrm{d}n\, \mathrm{d}s\, \mathrm{d}z \tag{A3}$$

where $\sigma_{zz}^{(k)}$, $\sigma_{sz}^{(k)}$, and $\sigma_{nz}^{(k)}$ are given in elsewhere.[9] Moreover, the virtual work can be written as

$$\delta W = \hat{M}_x \delta\theta_x(L, t) + \int_0^L [p_y(z, t)\delta v_0(z, t) + m_z(z, t)\delta\Theta(x, t)]\, \mathrm{d}z \tag{A4}$$

in which p_y and m_z are given by Eqs. (17) and (18), respectively. Carrying out the indicated integrations with respect to n and s, the kinetic energy can be reduced to the compact form

$$T = \frac{1}{2}\int_0^L [b_1\dot{v}_0'^2 + (b_4 + b_5)\dot{\Theta}^2 + (b_{10} + b_{18})(\dot{\Theta}')^2 + (b_{10} + b_{14})\dot{\theta}_x'^2]\,\mathrm{d}z \tag{A5}$$

where the various coefficients are given in previous work.[9,10] Similarly, using Eqs. (10), as well as the expressions

$$\begin{aligned} Q_y(z,t) &= \oint\left(N_{sz}\frac{\mathrm{d}y}{\mathrm{d}s} - N_{zn}\frac{\mathrm{d}x}{\mathrm{d}s}\right)\mathrm{d}s \\ M_x(z,t) &= \oint\left(yN_{zz} - L_{zz}\frac{\mathrm{d}x}{\mathrm{d}s}\right)\mathrm{d}s \\ M_z(z,t) &= 2\oint N_{sz}\psi\,\mathrm{d}s \\ B_\omega(z,t) &= \oint[F_\omega(s)N_{zz} + a(s)L_{zz}]\,\mathrm{d}s \end{aligned} \tag{A6}$$

in which Q_y is the one-dimensional stress resultant, M_x and M_z are stress couples, and B_ω is a bimoment,[10] and the two-dimensional constitutive equations

$$\begin{aligned} N_{zz}(s,z,t) &= K_{11}\epsilon_{zz}^0 + K_{12}\gamma_{sz}^0 + K_{13}\Theta' + K_{14}\epsilon_{zz}^n - \hat{N}_{zz} \\ N_{sz}(s,z,t) &= K_{21}\epsilon_{zz}^0 + K_{22}\gamma_{sz}^0 + K_{23}\Theta' + K_{24}\epsilon_{zz}^n \\ N_{zn}(s,z,t) &= A_{44}\gamma_{zn} \\ L_{zz}(s,z,t) &= K_{41}\epsilon_{zz}^0 + K_{42}\gamma_{sz}^0 + K_{43}\Theta' + K_{44}\epsilon_{zz}^n - \hat{L}_{zz} \\ L_{sz}(s,z,t) &= K_{51}\epsilon_{zz}^0 + K_{52}\gamma_{sz}^0 + K_{53}\Theta' + K_{54}\epsilon_{zz}^n \end{aligned} \tag{A7}$$

where K_{ij} denote the modified local stiffness coefficients[10] and $\hat{N}_{zz}$ and $\hat{L}_{zz}$ represent the piezoelectrically induced effects, and integrating with respect to n and s, the potential energy can be shown to have the form

$$\begin{aligned} V &= \frac{1}{2}\int_0^L [M_x\theta_x' + Q_y(\theta_x + v_0') - B_\omega\Theta'' + M_z\Theta']\,\mathrm{d}z \\ &= \frac{1}{2}\int_0^L [a_{33}(\theta_x')^2 + a_{55}\theta_x^2 + a_{66}(\Theta'')^2 + a_{77}(\Theta')^2 + a_{55}(v_0')^2 \\ &\quad + 2a_{37}\theta_x'\Theta' + 2a_{55}v_0'\theta_x + 2a_{56}\theta_x\Theta'' + 2a_{56}v_0'\Theta'']\,\mathrm{d}z \end{aligned} \tag{A8}$$

where the various coefficients can be found elsewhere.[10] Inserting Eqs. (A4), (A5), and (A8) into Eq. (A1) and carrying out the usual steps,[23] it is possible to obtain the boundary-value problem, Eqs. (12–14).

For practical reasons, it is necessary to discretize the boundary-value problem, which amounts to representing v_0, θ_x, and Θ by means of series of space-dependent trial functions multiplied by time-dependent generalized coordinates. The discretization can be more conveniently performed directly via the extended Hamilton's principle, Eq. (A1). To this end, we express the displacements v_0, θ_x, and Θ as follows:

$$\begin{aligned} v_0(z,t) &= \boldsymbol{\phi}_1^T(z)\boldsymbol{q}_1(t) \\ \theta_x(z,t) &= \boldsymbol{\phi}_2^T(z)\boldsymbol{q}_2(t), \qquad \Theta = \boldsymbol{\phi}_3^T(z)\boldsymbol{q}_3(t) \end{aligned} \tag{A9}$$

where

$$\begin{aligned} \boldsymbol{\phi}_1 &= [\phi_1 \quad \phi_2 \quad \cdots \quad \phi_N]^T \\ \boldsymbol{\phi}_2 &= [\phi_{N+1} \quad \phi_{N+2} \quad \cdots \quad \phi_{2N}]^T \\ \boldsymbol{\phi}_3 &= [\phi_{2N+1} \quad \phi_{2N+2} \quad \cdots \quad \phi_{3N}]^T \end{aligned}$$

are vectors of suitable trial functions and

$$\begin{aligned} \boldsymbol{q}_1 &= [q_1 \quad q_2 \quad \cdots \quad q_N]^T, \qquad \boldsymbol{q}_2 = [q_{N+1} \quad q_{N+2} \quad \cdots \quad q_{2N}]^T \\ \boldsymbol{q}_3 &= [q_{2N+1} \quad q_{2N+2} \quad \cdots \quad q_{3N}]^T \end{aligned}$$

are vectors of generalized coordinates. Then, inserting Eqs. (A9) into Eq. (A5), we can write the kinetic energy in the discrete form

$$T = \tfrac{1}{2}\dot{\boldsymbol{q}}^T M\dot{\boldsymbol{q}} \tag{A10}$$

where

$$M = \int_0^L \begin{bmatrix} b_1\boldsymbol{\phi}_1'\boldsymbol{\phi}_1'^T & 0 & 0 \\ 0 & (b_{10} + b_{14})\boldsymbol{\phi}_2'\boldsymbol{\phi}_2'^T & 0 \\ 0 & 0 & (b_4 + b_5)\boldsymbol{\phi}_3\boldsymbol{\phi}_3^T + (b_{10} + b_{18})\boldsymbol{\phi}_3'(\boldsymbol{\phi}_3')^T \end{bmatrix}\mathrm{d}z \tag{A11}$$

is the corresponding mass matrix and $\boldsymbol{q} = [\boldsymbol{q}_1^T \ \boldsymbol{q}_2^T \ \boldsymbol{q}_3^T]^T$ is the overall generalized displacement vector. Similarly, using Eq. (A8), the potential energy can be written as

$$V = \tfrac{1}{2}\boldsymbol{q}^T K\boldsymbol{q} \tag{A12}$$

in which

$$K = \int_0^L \begin{bmatrix} a_{55}\boldsymbol{\phi}_1'(\boldsymbol{\phi}_1')^T & a_{55}\boldsymbol{\phi}_1'\boldsymbol{\phi}_2^T & a_{56}\boldsymbol{\phi}_1'(\boldsymbol{\phi}_3'')^T \\ & a_{55}\boldsymbol{\phi}_2\boldsymbol{\phi}_2^T + a_{33}\boldsymbol{\phi}_2'(\boldsymbol{\phi}_2')^T & a_{37}\boldsymbol{\phi}_2'(\boldsymbol{\phi}_3')^T \\ \text{symmetric} & & a_{77}\boldsymbol{\phi}_3'(\boldsymbol{\phi}_3')^T + a_{66}\boldsymbol{\phi}_3''(\boldsymbol{\phi}_3'')^T \end{bmatrix}\mathrm{d}z \tag{A13}$$

is the corresponding stiffness matrix. Before we can discretize the virtual work, we recall from Eq. (15) that the boundary moment has the expression

$$\hat{M}_x = -k_p\dot{\theta}_x(L,t) \tag{A14}$$

where k_p is a control gain. Hence, inserting Eqs. (A9) and (A14) into Eq. (A4) and integrating with respect to z, the discretized virtual work can be expressed in the form

$$\delta W = -\dot{\boldsymbol{q}}^T H\delta\boldsymbol{q} + \boldsymbol{Q}^T\delta\boldsymbol{q} \tag{A15}$$

in which

$$H = -\begin{bmatrix} 0 & 0 & 0 \\ 0 & k_p\boldsymbol{\phi}_2(L)\boldsymbol{\phi}_2^T(L) & 0 \\ 0 & 0 & 0 \end{bmatrix} \tag{A16}$$

is a coefficient matrix and

$$\boldsymbol{Q} = \int_0^L [p_y\boldsymbol{\phi}_1^T \quad 0^T \quad m_z\boldsymbol{\phi}_3^T]^T\,\mathrm{d}z \tag{A17}$$

is a generalized force vector. Introducing Eqs. (A10), (A12), and (A15) in Eq. (A1), integrating with respect to time, and recognizing that $\delta \boldsymbol{q} = \boldsymbol{0}$ at $t = t_1, t_2$, we obtain the discrete equations of motion

$$M\ddot{\boldsymbol{q}}(t) + H\dot{\boldsymbol{q}}(t) + K\boldsymbol{q}(t) = \boldsymbol{Q}(t) \tag{A18}$$

A solution of Eq. (A18) can be obtained conveniently by casting it first in state form. To this end, we introduce the state vector $\boldsymbol{x} = [\boldsymbol{q}^T \quad \dot{\boldsymbol{q}}^T]^T$ and adjoin the identity $\dot{\boldsymbol{q}} \equiv \dot{\boldsymbol{q}}$. Then, the desired state form is

$$\dot{\boldsymbol{x}}(t) = A\boldsymbol{x}(t) + B\boldsymbol{Q}(t) \tag{A19}$$

where

$$A = \left[\begin{array}{c|c} 0 & I \\ \hline -M^{-1}K & -M^{-1}H \end{array}\right], \qquad B = \left[\begin{array}{c} 0 \\ \hline M^{-1} \end{array}\right] \tag{A20}$$

are coefficient matrices.

The homogeneous solution of Eq. (A19) has the exponential form

$$\boldsymbol{x}(t) = \boldsymbol{x}e^{\lambda t} \tag{A21}$$

in which $\boldsymbol{x}$ is a constant vector and λ a constant scalar, both generally complex. Inserting Eq. (A21) into Eq. (A19) with $\boldsymbol{Q} = \boldsymbol{0}$ and dividing through by $e^{\lambda t}$, we obtain the eigenvalue problem

$$A\boldsymbol{x} = \lambda \boldsymbol{x} \tag{A22}$$

which can be solved for the eigenvalues λ_r and eigenvectors $\boldsymbol{x}_r$ ($r = 1, 2, \ldots, 6N$), and we observe that if an eigensolution λ_s, $\boldsymbol{x}_s$ is complex, then the complex conjugate pair $\bar{\lambda}_s$, $\bar{\boldsymbol{x}}_s$ is also an eigensolution. The top half of the eigenvectors can be used to replace q_i in Eqs. (A9) so as to obtain the eigenfunctions corresponding to v_0, θ_x, and Θ.

To derive the particular solution, we first insert Eqs. (17) and (18) into Eq. (A17) and obtain the generalized force vector

$$\boldsymbol{Q}(t) = \int_0^L \left[F_0 \delta(z - z_0)\phi_1^T(z) \quad \boldsymbol{0}^T \quad F_0 x_0 \delta(z - z_0)\phi_3^T(z)\right] \mathrm{d}z e^{i\omega t} = \boldsymbol{Q}e^{i\omega t} \tag{A23}$$

where ω is the excitation frequency and

$$\boldsymbol{Q} = \left[F_0 \phi_1^T(z_0) \quad \boldsymbol{0}^T \quad F_0 x_0 \phi_3^T(z_0)\right]^T \tag{A24}$$

is a constant vector. Then, letting the particular solution of Eq. (A19) have the form

$$\boldsymbol{x}(t) = \boldsymbol{x}_p e^{i\omega t} \tag{A25}$$

we conclude that

$$\boldsymbol{x}_p = [i\omega I - A]^{-1}\boldsymbol{Q} \tag{A26}$$

in which I is the identity matrix. Equation (A26) can be used in conjunction with Eqs. (A9) to obtain frequency response plots corresponding to v_0 and Θ.

References

[1]Weisshaar, T. A., "Aeroelastic Tailoring–Creative Use of Unusual Materials," *Proceedings of the AIAA/ASME/ASCE/AHS 28th Structures, Structural Dynamics, and Materials Conference* (Monterey, CA), AIAA, New York, 1987 (AIAA Paper 87-0976).

[2]Lin, C. Y., and Crawley, E. F., "Aeroelastic Actuation Using Elastic and Induced Strain Anisotropy," *Journal of Aircraft*, Vol. 32, No. 5, 1995, pp. 1130–1137.

[3]Librescu, L., Meirovitch, L., and Song, O., "Integrated Structural Tailoring and Adaptive Materials Control for Advanced Aircraft Wings," *Journal of Aircraft*, Vol. 33, No. 1, 1996, pp. 203–213.

[4]Tzou, H. S., *Piezoelectric Shells, Distributed Sensing and Control of Continua*, Kluwer Academic, Dordrecht, The Netherlands, 1993.

[5]Baz, A., "Dynamic Boundary Control of Beams Using Active Constrained Layer Damping," *Proceeding of the Tenth VPI & SU Symposium* (Blacksburg, VA), edited by L. Meirovitch, 1995, pp. 49–64.

[6]Librescu, L., Song, O., and Rogers, C. A., "Adaptive Vibrational Behavior of Cantilevered Structures Modeled as Composite Thin-Walled Beams," *International Journal of Engineering Science*, Vol. 31, No. 5, 1993, pp. 775–792.

[7]Tzou, H. S., and Zhong, J. P., "Adaptive Piezoelectric Structures: Theory and Experiment," *Active Materials and Adaptive Structures, Materials and Structures Series*, edited by G. J. Knowles, Inst. of Physics, Bellingham, WA, 1992, pp. 219–224.

[8]Librescu, L., and Song, O., "Behavior of Thin-Walled Beams Made of Advanced Composite Materials and Incorporating Non-Classical Effects," *Applied Mechanics Reviews*, Vol. 44, No. 11, Pt. 2, 1991, pp. 174–180.

[9]Song, O., and Librescu, L., "Free Vibration of Anisotropic Composite Thin-Walled Beams of Closed Cross-Section Contour," *Journal of Sound and Vibration*, Vol. 167, No. 1, 1993, pp. 129–147.

[10]Librescu, L., Meirovitch, L., and Song, O., "Refined Structural Modeling for Enhancing Vibrations and Aeroelastic Characteristics of Composite Aircraft Wings," *La Recherche Aeospatiale*, No. 1, 1996, pp. 23–35.

[11]Maugin, G. A., *Continuum Mechanics and Electromagnetic Solids*, North-Holland, Amsterdam, 1988.

[12]Lottati, J., "Aeroelastic Stability Characteristics of a Composite Swept Wing with Tip Weights for an Unrestrained Vehicle," *Journal of Aircraft*, Vol. 24, No. 11, 1987, pp. 793–802.

[13]Librescu, L., and Simovich, J., "General Formulation for the Aeroelastic Divergence of Composite Swept Forward Wing Structures," *Journal of Aircraft*, Vol. 25, No. 4, 1988, pp. 364–371.

[14]Weisshaar, T. A., "Aeroelastic Stability and Performance Characteristics of Aircraft with Advanced Composite Swept Forward Wing Structures," U.S. Air Force Flight Dynamics Research Lab., Rept. AFFDL-TR-78-118, 1978.

[15]Librescu, L., and Thangjitham, S., "Analytical Studies on Static Aeroelastic Behavior of Forward-Swept Composite Wing Structures," *Journal of Aircraft*, Vol. 28, No. 2, 1991, pp. 151–157.

[16]Rehfield, L. W., and Atilgan, A. R., "Toward Understanding the Tailoring Mechanisms for Thin-Walled Composite Tubular Beams," *Proceedings of the First USSR–U.S. Symposium on Mechanics of Composite Materials* (Latvia SSR), edited by S. W. Tsai, J. M. Whitney, T.-W. Chou, and R. M. Jones, American Society of Mechanical Engineers, New York, 1989, pp. 187–196.

[17]Smith, E. C., and Chopra, I., "Formulation and Evaluation of an Analytical Model for Composite Box-Beams," *Journal of the American Helicopter Society*, Vol. 36, No. 3, 1991, pp. 23–35.

[18]Lagnese, J. E., and Lions, J. L., "Boundary Stabilization of Thin Plates," *Collection RMA*, Masson, Paris, 1988.

[19]Lagnese, J. E., "Boundary Stabilization of Thin Plates," SIAM *Studies in Applied Mechanics*, Vol. 10, edited by M. Slemrod, Society for Industrial and Applied Mathematics, Philadelphia, 1989.

[20]Crawley, E. F., "Intelligent Structures for Aerospace: A Technology Overview and Assessment," *AIAA Journal*, Vol. 31, No. 8, pp. 1689–1699, 1994.

[21]Bailey, T., and Hubbard, J. E., Jr., "Distributed Piezoelectric-Polymer Active Vibration Control of a Cantilever Beam," *Journal of Guidance, Control, and Dynamics*, Vol. 8, No. 5, 1985, pp. 605–611.

[22]Berlincourt, D. A., Curran, D. R., and Jaffe, H., "Piezoelectric and Piezomagnetic Materials and Their Function in Transducers," *Physical Acoustics—Principles and Methods*, edited by E. P. Mason, Vol. 1, Pt. A, Academic, New York, 1964, pp. 202–204.

[23]Meirovitch, L., *Principles and Techniques of Vibrations*, Prentice–Hall, Englewood Cliffs, NJ, 1997.

[24]Meirovitch, L., and Seitz, T. J., "Structural Modeling for Optimization of Low Aspect Ratio Composite Wings," *Journal of Aircraft*, Vol. 32, No. 5, 1995, pp. 1114–1123.

[25]Librescu, L., and Song, O., "On the Static Aeroelastic Tailoring of Composite Aircraft Swept Wings Modelled as Thin-Walled Beam Structures," *Composite Engineering*, Vol. 2, Nos. 5–7 (Special Issue: Use of Composites in Rotorcraft and Smart Structures), 1992, pp. 497–512.

[26]Karpouzian, G., and Librescu, L., "Three-Dimensional Flutter Solution of Aircraft Wings Composed of Advanced Composite Materials," *Proceedings of the AIAA/ASME/ASCE/AHS/ASC 35th Structures, Structural Dynamics, and Materials Conference*, AIAA, Washington, DC, 1994, pp. 2851–2856 (AIAA Paper 94-1490).

R. K. Kapania
Associate Editor